Available online at www.sciencedirect.com
SCIENCE DIRECT®
Journal of Power Sources 125 (2004) 70–76
JOURNAL OF POWER SOURCES
www.elsevier.com/locate/jpowsour

Electrochemical intercalation of lithium into graphite–antimony composites synthesized by reduction of a $SbCl_5$–graphite intercalation compound by gaseous caesium

A. Dailly [a], J. Ghanbaja [a], P. Willmann [b], D. Billaud [a,*]

[a] *LCSM, UMR CNRS 7555, UHP Nancy I, BP 239, 54506 Vandoeuvre-les-Nancy Cedex, France*
[b] *CNES, 18 Avenue E. Belin, 31055 Toulouse Cedex, France*

Received 19 December 2002; received in revised form 1 July 2003; accepted 3 July 2003

Abstract

Preparation of antimony-based graphite composite using a graphite intercalation compound as precursor was described. A $C_{12}SbCl_5$ graphite intercalation compound was reduced by caesium in the vapor phase at 70 °C. The resulting compound was composed of antimony particles deposited on a graphite matrix. Used as negative-electrode material for lithium-ion rechargeable cells, this composite presented not only an improved storage capacity (490 mAh g^{-1} between 0 and 2 V versus Li^+/Li) by comparison with free graphite but also enhanced dimensional stability of lithium–antimony alloys.

Keywords: Graphite intercalation compound; Lithium-ion battery; Antimony

1. Introduction

Many metals such as Al, Sn, Bi, Sb, etc., which can reversibly alloy with lithium have shown a renewal of interest as potential negative-electrode materials for lithium-ion batteries. Indeed, lithium storage metals have been studied long before carbonaceous materials were chosen for the same application [1]. Although lithium alloys present theoretical specific charge much higher than those of the commonly used lithiated carbon materials, their use has been hindered by significant volume variation occurring during lithium insertion and removal. The strong volume expansion leads to mechanical stresses including a rapid decay of the mechanical stability and cycle life of the electrode. This latter suffers from crumbling and cracking which cause its fast disintegration. In order to counteract the mechanical degradation, small particle size materials and composites materials containing active/inactive phases have been investigated. With regard to a first concept, the superfine alloys use, thanks to the small absolute changes in the particle dimensions, allows to improve cyclic performances compared with pure metal or alloy with large particle size. Another concept consists in the dispersion of small particles of reactive lithium alloys with less active or inert phases. The more electroactive particles can expand during the alloying into ductile surroundings of still unreacted materials. The amorphous tin composite oxide (TCO) anodes patented by Fujifilm exemplify such an approach [2]. The high reversible capacity and the excellent cyclability of TCO can be attributed to the presence of a Sn nano-structured active phase as finely dispersed in a network of Li_2O, formed upon the first charge, and glass formation promoters that hinder the aggregation of Sn particles.

Several host materials with enhanced performance have also been proposed as alternative anode [3–5] such as intermetallic lithium insertion compounds, where lithium occupies interstitial sites giving only a small volume expansion, or mixed active material composites where stepwise lithium insertion mode into the different active phases buffers the host volume expansion. A successful example is the $SnSb_x$ compound [3].

Processes have been developed to incorporate metal particles in a conductive matrix capable of reversible insertion/removal of lithium like carbon or graphite. Not only a substrate, which is an active lithium-storage compound, allows to add to the overall capacity of the composite material but it also provides a mechanical and conductivity support for the dispersed phase [6,7]. Tin was used as the attractive element in these whole attempts because it can combine with lithium to form $Li_{22}Sn_5$ alloys with a theoretical capacity of 990 mAh g^{-1}.

* Corresponding author. Tel.: +33-3-8368-4622; fax: +33-3-8368-4623.
E-mail address: billaud@lcsm.uhp-nancy.fr (D. Billaud).

0378-7753/$ – see front matter © 2003 Elsevier B.V. All rights reserved.
doi:10.1016/S0378-7753(03)00825-5

In this study, we examine the feasibility to incorporate metal particles between graphene layers by using graphite intercalation compounds (GICs) as precursors materials. The insertion of such metals in a spontaneous way is impossible. Elements which intercalate spontaneously into the graphite are electropositive elements: alkaline metals, alkaline earth metals and bivalent, rather volatile lanthanides [8]. Thereby, metal introduction into graphite can be led only by indirect way as for example the chemical reduction of a metal compound, generally a beforehand intercalated metal halide, between graphene layers. The considered reduction process consists in reducing an antimony pentachloride graphite intercalated compound with caesium in the vapor phase. The choice turned to the antimony because, on one hand, it is rather easy to synthesize graphite intercalation compounds with antimony-based compounds, particularly antimony pentachloride [9,10], and on the other hand, antimony–lithium alloys present high theoretical specific charge (Li_3Sb: 660 mAh g^{-1}). Processes based on the chemical reduction of acceptor graphite transition metal chloride compounds with alkaline metal phase have been tested with the aim to prepare intercalated metal. With some metals, attempts have been revealed decisive because insertion or inclusion graphite compounds with these last ones were obtained [11,12]. In many other cases, the metal chloride reduction occurs mainly outside graphite layers and a dispersion of metal particles on the graphite surface is observed. In our knowledge, there was no attempt of $SbCl_5$ reduction with vapor phase alkali metal, beforehand, intercalated into graphite. In this paper, we present the results obtained after reduction of a $C_{12}SbCl_5$ graphite intercalation compound by caesium in the vapor phase. The resulting products, characterized by X-ray diffraction and transmission electron microscopy, were then tested as negative-electrode materials for lithium-ion batteries.

2. Experimental

$SbCl_5$–graphite intercalation compounds used in this investigation may be conveniently prepared in the vapor phase by the two-bulb method in which the graphite sample is maintained at a temperature T_g which is higher than the $SbCl_5$ temperature T_i. Initial conditions for intercalation were established by using the conditions of Melin and Herold [13]. In the present experiment, the intercalant temperature was held constant at 165 °C while the host material, Ceylon powder with 25–45 μm average size, was maintained at 170 °C during 12 h.

The reduction of the as-synthesized first-stage compound $C_{12}SbCl_5$ by caesium in the vapor phase was then performed with a small temperature gradient between the alkali metal ($T_{Cs} = 70$ °C) and the material for about 1 month. Caesium was introduced in excess into the reactor so that the $SbCl_5$ reduction might be complete.

Phases were identified via X-ray diffraction using an automated powder diffractometer with Kα radiation (Rotaflex RU-200B, RIGAKU generator and CPS 120 INEL detector, transmission assembly) with a holder appropriate for air-sensitive materials. Samples were prepared under argon gas by inserting some powder into Lindemann glass capillaries which were then sealed after glove box transfer. Diamond, added to the GIC sample, was used as an internal reference. The electron microscopy observations were obtained using a Philips CM20 instrument operated at 200 kV. Samples were prepared by previously dispersing in tetrahydrofuran, picking up a drop of the sonicated suspension of the Sb-based graphite compound and then depositing on a carbon grid.

Electrochemical tests were performed using lithium acting both as reference and counter electrode in a laboratory-type glass cell. A 1-methyl-2-pyrrolidinon slurry of 95 wt.% of Sb-based graphite anode material and 5 wt.% of polyvinylidene fluoride (PVDF) was used to coat a thick copper current collector. $LiClO_4$ (1 M) in ethylene carbonate (EC) was used as an electrolyte. All of the test cells were assembled in an argon atmosphere and cycled using a Mac Pile II, potentiostat–galvanostat (Biologic) working either in the voltammetry mode between 0 and 2 V versus Li^+/Li with following steps of 2.5 mV every 2 min or in the galvanostatic mode with a constant current density for charge and discharge of 7 μA mg^{-1} between 0 and 2 V versus Li^+/Li. Current was applied for 6 min and the circuit was then opened for 10 s.

3. Results and discussion

The XRD patterns from the antimony pentachloride graphite intercalation compound before (a) and after (b) its reduction by caesium in the vapor phase are displayed in Fig. 1. X-ray diffraction results from the GIC provide averaged informations on the chemical composition ($C_{12}SbCl_5$ stage 1) and the interplanar distance ($d_i = 942$ pm). Few un-assigned peaks can be attributed to h k 0 or h k l reflections [9,13]. The diffraction pattern obtained after reduction consists of up to 10 fine lines, which were well indexed to CsCl, and a broad peak corresponding to deintercalated graphite. X-ray reflections of the pristine material are no more present. The weak intensity and the broadening of the 0 0 2 graphite reflection reveal a strong structural disorder involved by deintercalation and further reduction processes. The coherence length (size of the coherent domains) along the *c*-direction of graphite, L_C, was evaluated from the half height width of the 0 0 2 reflection using the Scherrer equation; it is equal to 11 nm. This value can differ according to the samples. The sharp peaks corresponding to the cubic system of the crystalline byproduct CsCl, tend to hide any other reflection which could belong to antimony assuming this metal be crystallized. So the samples were washed with H_2O/C_2H_5OH mixture in order to remove CsCl from the

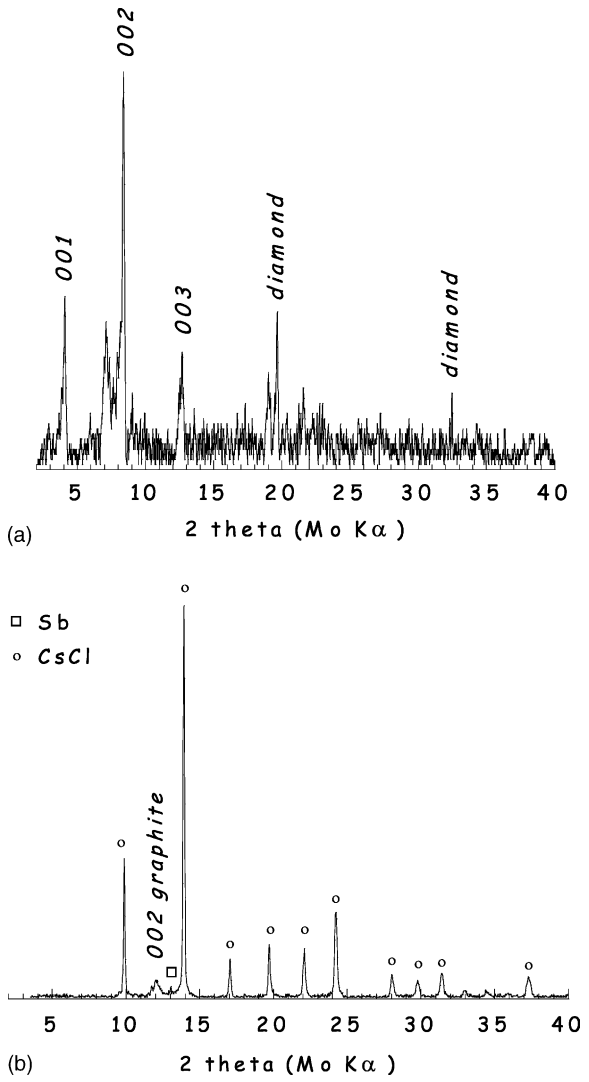

Fig. 1. XRD patterns of antimony pentachloride intercalated graphite compound (a) before and (b) after reduction by gaseous caesium.

surface. The XRD results of the washed sample are presented in Fig. 2: they reveal an important removal of CsCl evidenced by the decrease of the intensity of CsCl reflections compared to the 0 0 2 reflection of graphite. Though there was no detectable reflections of metallic antimony on the X-ray diffraction pattern, a more direct analysis of the sample was performed by EDX and ensured that this element was present in the material (Fig. 3a). In the case of the as-synthetized composite strong lines due to Sb and Cs, on one hand, and weak lines due to Cl, on the other hand, were detected in the energy dispersive spectrum. The presence of an important quantity of caesium is due to its introduction with excess in the reactional medium. The EDX spectrum obtained with the sample washed with H_2O/C_2H_5OH mixture (Fig. 3b) exhibited exclusively strong peaks due to Sb while no peak for Cl and Cs were present. From the selected area electron diffraction (SAED) pattern displayed in Fig. 4, CsCl reflections appear as dotted rings

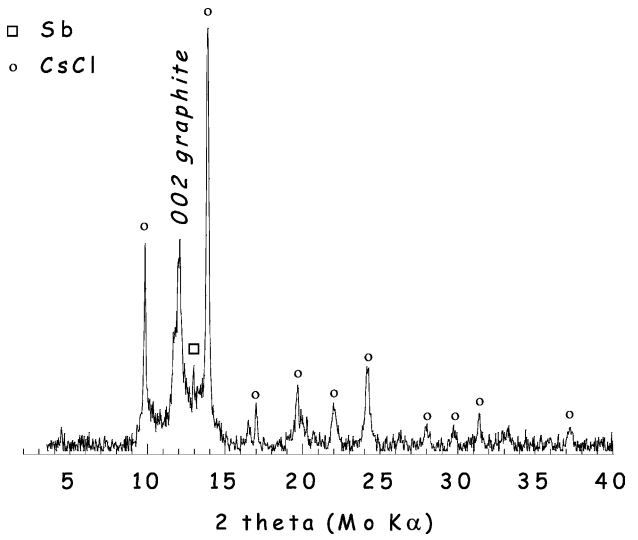

Fig. 2. XRD pattern of the washed reduced product with H_2O/C_2H_5OH mixture.

superimposed to the h k 0 spots related to pristine graphite. Besides these reflections, a weak intensity ring corresponds to the maximum relative intensity of the 0 1 2 reflection of antimony. The absence of thin and intense rings in the electron diffraction pattern demonstrates that antimony is

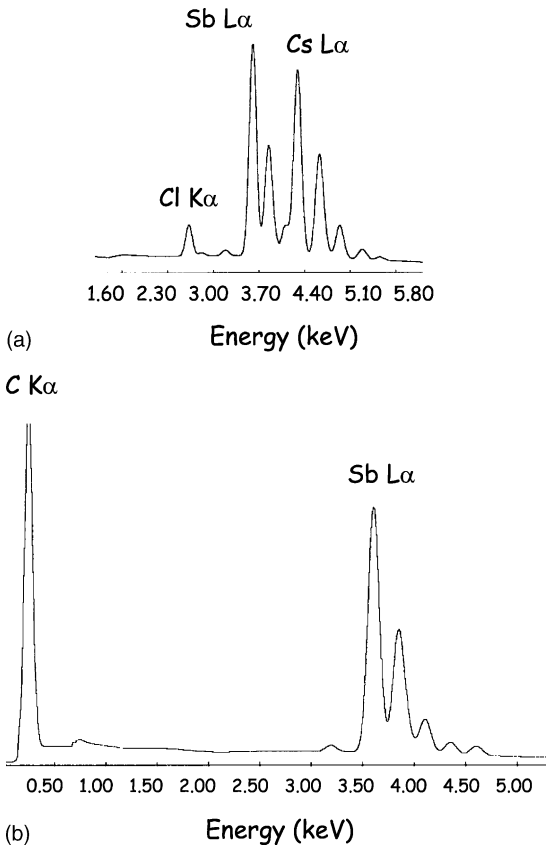

Fig. 3. EDX spectra of (a) the non-washed reduced product obtained after $C_{12}SbCl_5$ reduction by gaseous caesium and (b) the washed material.

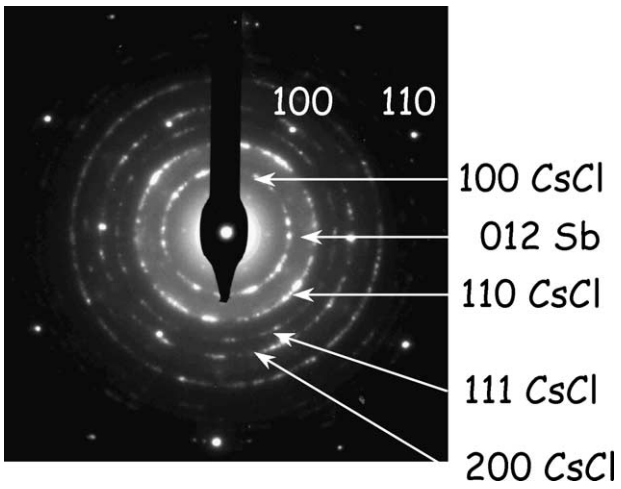

Fig. 4. SAED pattern of the non-washed antimony-based graphite compound.

amorphous. These results corroborate those of XRD. Bright-field micrographs displayed in Fig. 5 clearly illustrate the complexity of the microstructure in which both crystallite and amorphous particles are present. In the non-washed samples, the particle distribution is inhomogeneous. Not only metallic antimony clusters and CsCl crystals are supported on graphite surface (Fig. 5a) but also shapeless free nodules (Fig. 5b) and well-crystallized antimony particles (Fig. 5c) were evidenced. We could suggest that the conditions of reaction such as temperature and reducing agent nature govern the structure and the dispersion of the particles. TEM was also employed to characterize the structure of the washed sample. Bright-field micrographs of the washed sample (Fig. 6) show a film-like deposit of small antimony particles on graphite surface. Antimony appears also present as shapeless independent particles. Considering all these observations, we can conclude that the alkali metal vapor is a

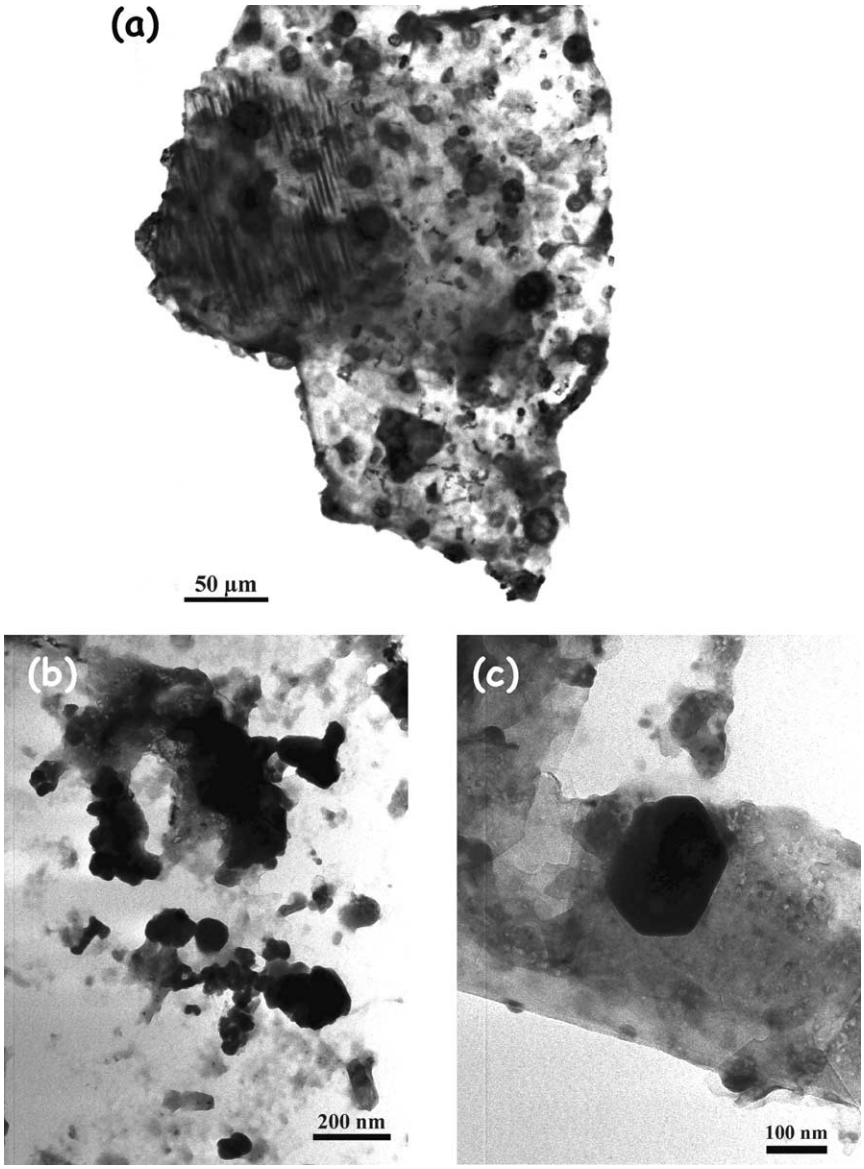

Fig. 5. Bright-field micrographs of supported particles and free nodules of antimony present in the non-washed reduced compound.

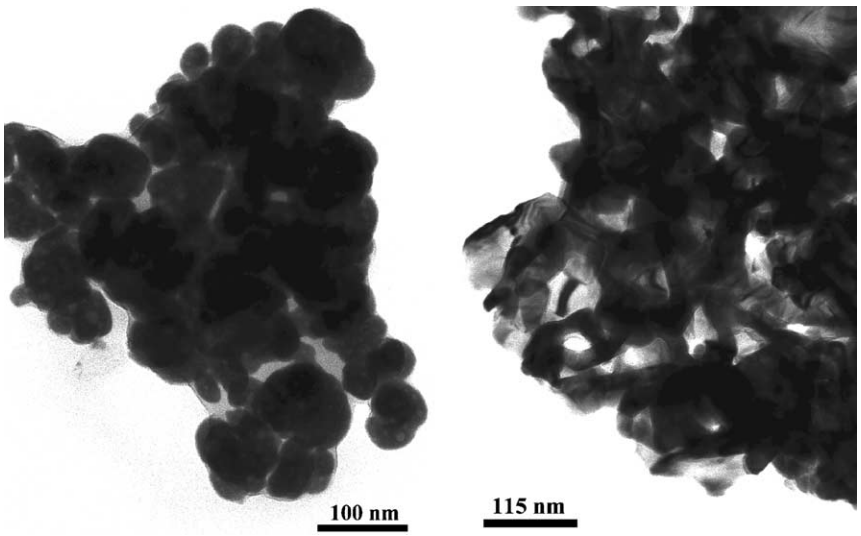

Fig. 6. Bright-field micrographs related to antimony distribution in the washed material.

good reducing agent for intercalated metal halides due to its advantage to be intercalated into graphite. That could favor the reduction of $SbCl_5$ between the graphene layers to form either intercalated or included antimony. In the first case, a partial charge transfer occurred with formation of intercalated $Sb^{\delta+}$ while in the second case, only neutral antimony is present between the graphene sheets. However, antimony particles are mainly present at the edges of the graphite layers. The mobilities of both intercalated Cs and $SbCl_5$ are so important that the reduction of $SbCl_5$ occurs after its deintercalation. Generated antimony particles were aggregated and distributed heterogeneously through the whole material. Metallic clusters were mainly supported on the graphite matrix which seemed to be strongly distorted due to the fast $SbCl_5$ deintercalation. Morphological and structural characteristics of the antimony particles were preserved after washing. This result is consistent with the fact that antimony is not readily attacked by water and that it is passivated in air and moisture at room temperature.

Electrochemical tests have been carried out by using as negative-electrode material either non-washed or washed Sb-based graphite composite. Fig. 7 exhibits the first cyclic voltammograms for these electrodes. A weak intensity shoulder around 1.5 V was present in the voltammogram related to the first reduction of the washed sample. It might be interpreted as the reduction of oxidized antimony. Indeed, the formation of Li_2O from a convertible oxide is well documented in the SnO system [2,14] but is also quoted for antimony oxides [15]. This irreversible reaction occurs in the early stages of the first cycle. It is followed by the alloying of the remaining lithium with the elemental antimony. In the subsequent cycles, the lithium is reversibly alloyed with antimony while Li_2O remains inactive. The formation of small amounts of antimony oxides probably occurs during the sample washing. Both for non-washed and washed samples, a consequent negative current is observed down

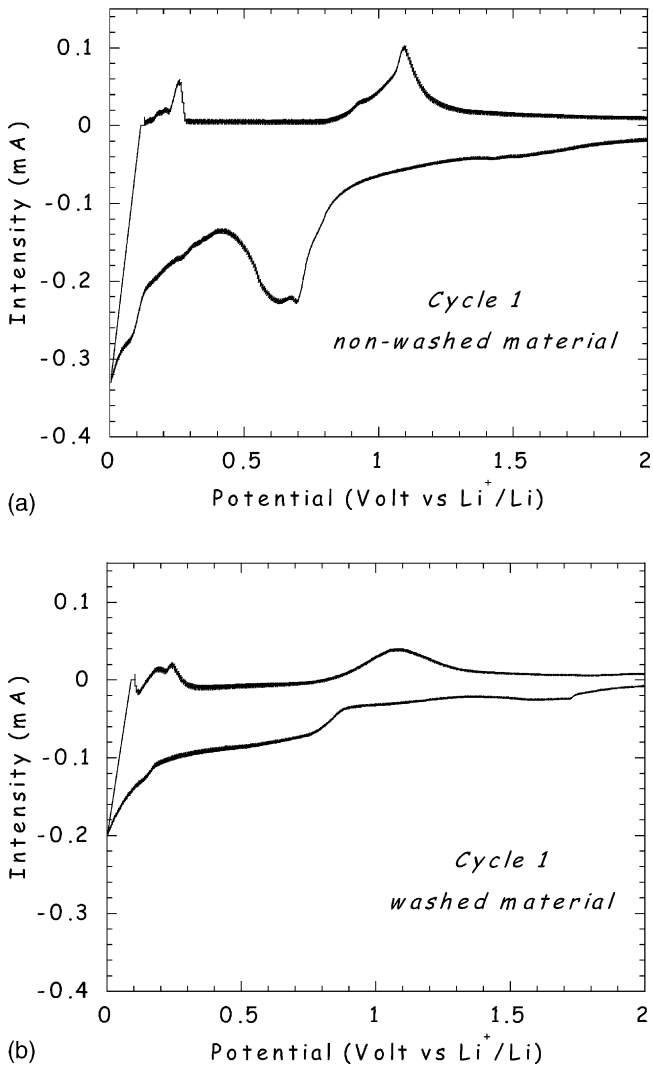

Fig. 7. Cyclic behavior of the non-washed and washed antimony-based graphite compounds.

about 0.9 V. A broad peak centered around 0.6 V is evidenced in the reduction part of the voltammogram of the non-washed material. This reduction current could be attributed to various reactions: a first one is the formation of a solid-electrolyte interphase (SEI) appearing both on carbon materials and lithium storage metals [16]. This passivation layer is expected to form through a side reaction of partial electrolyte decomposition; another one should correspond to the simultaneous insertion of lithium into antimony [17,18]. This hypothesis was supported by the presence of a peak in the oxidation process for a potential value close to 1.0 V, which gives evidence for the reversibility of lithium alloying. Contrary to the metal, graphite presents in the first cycles, a poor reversibility of the lithium intercalation. Indeed, to the present intense peak observed during the reduction at the lowest potentials corresponds a weak and badly defined peak in oxidation. Obviously, the important structural disorganization of the graphite observed after its de-intercalation would imply difficulties for intercalating lithium in a reversible way. The graphite exhibited however a more classic behavior up to the fifth voltammetric cycle illustrating an improved accessibility of lithium between these graphene layers. Our graphite–antimony materials present a good cyclability and stability both for the metal and the graphite matrix throughout the duration of the experiment as shown in Fig. 8 which compares the 5th and 20th voltammograms related to the washed materials. The intensity profiles decay only very slowly during the cycling. The electrochemical behavior of the non-washed product is similar. A plot of the cycle life of the washed Sb-based graphite composite is shown on Fig. 9. Galvanostatic results were obtained with a sample which was previously cycled 20 times in slow scan voltammetry mode The charge and discharge curves for the 40th cycle displayed in the inset of Fig. 9 exhibit various plateaux which provide evidence of the reaction mechanisms: firstly, lithium alloying with antimony occurs near 0.8 V versus Li^+/Li; then the extended flat voltage profile near 0 V versus Li^+/Li is indicative of the formation of lithium graphite intercalation compounds.

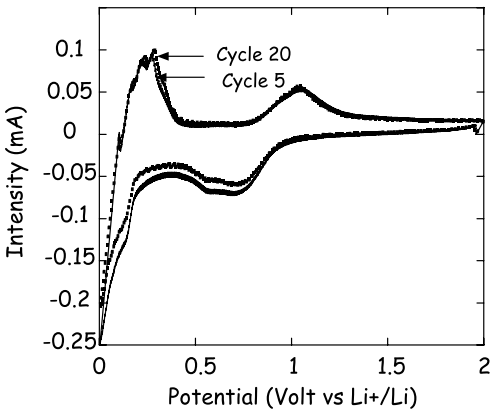

Fig. 8. Selected cyclic voltammograms of the washed Sb–graphite composite.

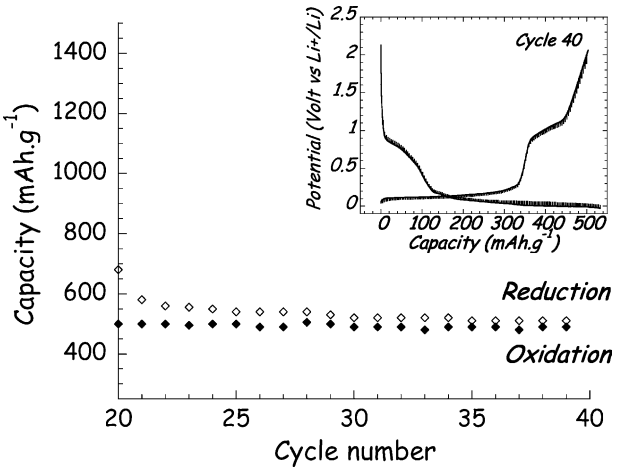

Fig. 9. Cycle life of the washed product after 20 voltammetric cycles and voltage profile of the 40th cycle.

Both processes were reversible. Cycles 20–40 give evidence for a stable specific capacity of approximately 490 mAh g^{-1} in which 160 mAh g^{-1} can be attributed to the metal. Assuming that the final middle composition be close to $C_{12}Sb$ implies that the material contains 46 wt.% Sb. Such a metal concentration would lead to a theoretical mass capacity of $\approx$504 mAh g^{-1}, based on the assumption of full lithiation of the Sb–graphite composite of the given composition to Li_3Sb and LiC_6, which agrees with the experimentally evaluated reversible capacity. The small difference could be explained by the fact that the given composition of the graphite intercalation compound, $C_{12}SbCl_5$, is a theoretical average composition [13]. Moreover, $SbCl_5$ was supposed to be completely reduced into metallic Sb. Only elemental analyses of the composites could give the exact compositions of the samples, especially the Sb/C ratio. Even if the metal particles are not included between the graphite layers, they present a large stability throughout the cycling. Compared to bulk antimony, which has essentially no cycle life [20], our as-synthesized Sb–graphite composite exhibits far superior electrochemical performances during charge and discharge cycling. To our knowledge, no investigation about antimony expects such results. The metal has not only seemed to undergo the mechanical constrains which arise generally during Li^+ insertion and Li^+ removal, but when associated to graphite in our synthesis conditions, it provides to the Sb–graphite composite a large improvement of the specific charge.

4. Conclusion

A novel process has been described to synthesize a negative-electrode composite material for rechargeable lithium-ion batteries. In such a material, lithium alloying antimony particles are formed after reduction of intercalated antimony pentachloride by gaseous caesium. The resulting reduced material is composed of aggregated antimony

nanoparticles supported and possibly bonded to the graphite matrix. Combining the high lithium storage capacity of the semi-metal antimony and the stable cyclability of graphite results in an improved and almost stable capacity. With Li–Sb alloys synthesized by classical ways, the electrode pulverization occurs generally during the charge and discharge processes [20]. To the contrary, in the Sb–graphite composites obtained by reduction of $SbCl_5$–graphite intercalation compounds by caesium, such an electrode pulverization does not occur significantly. We can hypothesize that this reduction method leads to materials in which antimony is possibly bonded to graphite. The nature of this bond is not clear at the present time but it appears strong enough to avoid the dramatic effects related to the large volume variations occurring during antimony alloying. Graphite provides not only a mechanical and a conducting support for the dispersed Sb phase that it allows the particles to remain electrically connected but it is also by itself electrochemically active towards Li^+ insertion and removal. The origin of the metal–graphite interaction, supposed to be a key point for long life cycling, is being currently studied by comparing the properties of selected metal–graphite systems composed of various metals and graphites [19].

References

[1] M. Winter, J.O. Besenhard, M.E. Spahr, P. Novak, Adv. Mater. 10 (10) (1998) 725–763.
[2] Y. Idota, T. Kubota, A. Matsufuji, Y. Maekawa, T. Miyasaka, Science 726 (1997) 1395–1397.
[3] J. Yang, Y. Takeda, N. Imanishi, J.Y. Xie, O. Yamamoto, Solid State Ionics 133 (2000) 189–194.
[4] K.C. Hewitt, L.Y. Beaulieu, J.R. Dahn, J. Electrochem. Soc. 148 (5) (2001) A402–A410.
[5] X.B. Zhao, G.S. Cao, Electrochim. Acta 46 (2001) 891–896.
[6] J.Y. Lee, R. Zhang, Z. Liu, J. Power Sources 90 (2000) 70–75.
[7] J. Read, D. Foster, J. Wolfenstine, W. Behl, J. Power Sources 96 (2001) 277–281.
[8] A. Hérold, NATO Advanced Science Institute series special program on condensed systems of low dimensionality, in: A.P. Legrand, S. Flandrois (Eds.), Chemical Physics of Intercalation, Plenum Press, New York, 1987.
[9] J. Mélin, A. Hérold, C.R. Acad. Sci., Paris 269 (1969) 877–883.
[10] H. Homma, R. Clarke, Phys. Rev. B 31 (9) (1985) 5865–5877.
[11] M. Ohira, A. Messaoudi, M. Inagaki, F. Béguin, Carbon 29 (8) (1991) 1233–1238.
[12] A.T. Shuvayev, B.Yu. Helmer, T.A. Lyubeznova, V.L. Kraizman, A.S. Mirmilstein, L.D. Kvacheva, Yu.N. Novikov, M.E. Volpin, J. Phys. France 50 (1989) 1145–1151.
[13] J. Melin, A. Herold, Carbon 13 (5) (1975) 357–362.
[14] R.A. Huggins, Solid State Ionics 115 (1998) 57–67.
[15] H. Li, X. Huang, L. Chen, Solid State Ionics 123 (1999) 189–197.
[16] M. Wachtler, J.O. Besenhard, M. Winter, J. Power Sources 94 (2001) 189–193.
[17] J. Wang, I.D. Raistrick, R.A. Huggins, J. Electrochem. Soc. 133 (1983) 457–460.
[18] R. Alcantara, F.J. Fernandez-Madrigal, P. Lavela, J.L. Tirado, J.C. Jumas, J. Olivier-Fourcade, J. Mater. Chem. 9 (1999) 2517–2521.
[19] L. Balan, A. Dailly, D. Billaud, to be published.
[20] W.X. Chen, J.Y. Lee, Z. Liu, Carbon 41 (2003) 966.